

Standardization of type Ia supernovae

**Rodrigo C V Coelho, Maurício O Calvão, Ribamar R R Reis
and Beatriz B Siffert**

Instituto de Física, Universidade Federal do Rio de Janeiro, Av. Athos da Silveira
Ramos 149, 21941-972, Rio de Janeiro, RJ, Brazil

Abstract. Type Ia supernovae (SNe Ia) have been intensively investigated due to its great homogeneity and high luminosity, which make it possible to use them as standardizable candles for the determination of cosmological parameters. In 2011, the physics Nobel prize was awarded “for the discovery of the accelerating expansion of the Universe through observations of distant supernovae.” This a pedagogical article, aimed at those starting their study of that subject, in which we dwell on some topics related to the analysis of SNe Ia and their use in luminosity distance estimators. Here we investigate their spectral properties and light curve standardization, paying careful attention to the fundamental quantities directly related to the SNe Ia observables. Finally, we describe our own step-by-step implementation of a classical light curve fitter, the stretch, applying it to real data from the Carnegie Supernova Project.

PACS numbers: 95.36.+x, 97.60.Bw, 98.80.Es

Keywords: Cosmology, type Ia supernova, dark energy, light curve standardization

1. Introduction

A supernova (SN or SNe, from the plural *supernovae*) is a stellar explosion which may occur at the final stage of the evolution of a star or as the result of the interaction between stars in a binary system. The current supernova classification follows the historical order in which these events were observed. Initially, the explosions were divided into types I and II, according to the presence (type II) or absence (type I) of hydrogen emission lines in their spectra. Later, the observation of SNe with different spectral features resulted in the introduction of the subtypes which we use nowadays (see figure 1). SNe of types II, Ib and Ic are now believed to occur due to gravitational collapse of massive stars (above ~ 8 solar masses), which leave behind a neutron star or a black hole. Type Ia SNe, on the other hand, are believed to be thermonuclear explosions in which the star is completely incinerated. It is currently accepted that SN Ia are thermonuclear explosions [1] of carbon-oxygen white dwarfs that reach explosion conditions when, by accreting mass

from a companion, approach the Chandrasekhar limiting mass (~ 1.4 solar masses) \ddagger . [3] In the single degenerate scenario, the companion is generally considered to be a main sequence, a red giant or an AGB star, whereas in the double degenerate scenario it is another white dwarf. The nitty-gritty details of the explosion process and the progenitor channel are still open to debate, both theoretically and observationally. [4, 5, 6]

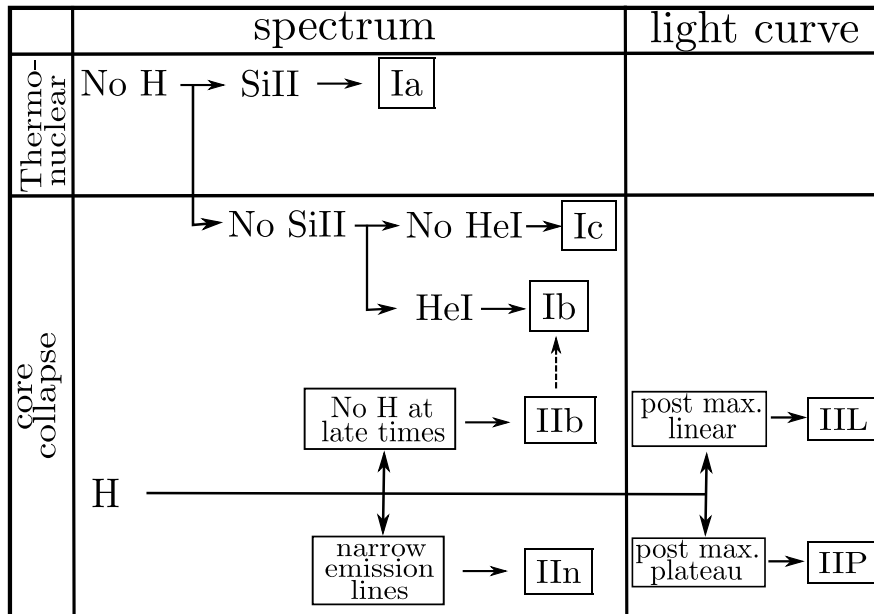


Figure 1. Schematic classification of supernovae.

As already stated, SNe are classified according to the presence or absence of certain spectral lines in their spectra and, for SNe II subtypes, the shape of their light curves. Type I SNe can be divided into three subtypes: SNe Ia present a silicon absorption feature around wavelength $\lambda = 6150 \text{ \AA}$ (their main characteristic); SNe Ib does not present silicon lines but present helium absorption lines; and SNe Ic present neither silicon nor helium features. To learn more about the spectral features of SNe, see [7]. The most interesting subtype for cosmological purposes is the Ia, because of their high power, which allows us to detect them in distant galaxies, and their quite homogeneous emission, which makes possible their use as standard candles.

A given class of astrophysical objects (or events) is considered a standard candle when their intrinsic luminosity is known or can somehow be estimated. In the case of SNe Ia, the observation of nearby events showed that all explosions had quite similar luminosities and the relatively small variations (as compared to the typical magnitudes of SNe Ia) can be corrected for (in fact, due to the existence of such fluctuations these events should actually be considered *standardizable* candles). SNe Ia themselves can be divided into subgroups and a classification scheme much used in the literature is the

\ddagger The exact value of this limiting mass depends on several properties of the white dwarf: metallicity, Coulomb corrections, temperature, rotation, magnetic fields, etc; in any event, realistically, these corrections seem to amount to no more than 10%. [2]

one by Branch *et al.*,[8] according to which these events can be 1991bg-like§, which are subluminoous, 1991T-like, which are superluminoous, and normal (*Branch-normal*). To have concrete numbers to express those variations, we calculated the sample standard deviation in absolute magnitudes M_B (cf. section 2) of the SNe Ia in a sample of Vaughan *et al.*,[9] comprising 50 SNe Ia, of which 25 are Branch-normal. Considering only the Branch-normal SNe Ia, the standard deviation of the distribution of M_B is 0.65 mag, while its mean is -18.5 mag. For a more recent data sample, see [10] Since the flux of a source measured on Earth is proportional to the source’s luminosity and inversely proportional to its distance squared (more precisely, to its luminosity distance squared, which we will define later), we see that it is possible to estimate the SNe Ia distance by measuring its flux.

It was using SNe Ia that the winners of the 2011 physics Nobel prize discovered in 1998 and 1999 that the universe is currently on an accelerated expansion.[11, 12] Currently, we believe that the cosmic acceleration is caused, in the context of general relativity, by an unknown form of energy, called dark energy, which would generate a gravitational repulsion unlike radiation, baryonic and cold dark matter, for which the gravitational interaction is attractive. The most popular candidate for dark energy is the cosmological constant, which is usually interpreted as vacuum energy. There are, nevertheless, other explanations for the accelerated expansion being investigated, based either on modifications of general relativity, or on the existence of inhomogeneities in the matter distribution of the Universe.[13]

As already mentioned, SNe Ia are standardizable candles which can be observed in very distant galaxies due to their high power. They are, however, rare events || and, since being explosions, they are transients (lasting around three months), which makes their observation a difficult task. In order to detect a high number of SNe, various projects are being planned, as this will demand a greater number of researchers in the field. For a list of these projects and some of the most important past and present experiments, see Table 1. Our goal in this work is to highlight some basic concepts concerning the use of SNe Ia for cosmology, which we found are not detailed in textbooks. We believe that this work will be of great utility for those who are starting their research in the field, as well as for researchers who have never worked specifically in this field.

In section 2 we present the basic concepts of spectrum, light curve, flux, magnitudes, all of them derivable from the fundamental concept of specific flux. In section 3, we discuss the influences distance and redshift have on the specific flux of an arbitrary source. In section 4 we discuss our naive light curve standardization, by taking advantage of a sort of stretch correction that characterizes only the variations in SNe Ia rise-and-decline rates, but not the intrinsic luminosity differences. In section 5 we present our

§ Supernovae are named for their year of occurrence and an uppercase letter, e.g., “SN 1987A”. If the alphabet is exhausted, double lower case naming is used: [Year] aa .. az, ba .. bz, etc; e.g., “SN 1997bs”.

|| For supernovae relatively close to our galaxy with $0 < z < 0.3$, the rate of occurrence of SNe Ia per volume is $(3.43 \pm 0, 15) \times 10^{-5}$ supernovae/year/Mpc³, according to [14].

Table 1. Past, current and future experiments to detect SNe: Equation of State: SupErNovae trace Cosmic Expansion (ESSENCE) [15], Supernova Legacy Survey (SNLS) [16], Sloan Digital Sky Survey (SDSS) [17], Panoramic Survey Telescope & Rapid Response System (Pan-STARRS) [18], Dark Energy Survey (DES) [19], Javalambre Physics of the Accelerating Universe (J-PAS) [20] and Large Synoptic Survey Telescope (LSST) [21]. The third column gives the number of spectroscopically confirmed SNe Ia for past experiments and the total number of expected detections for current and future ones.

Name	Running period	# of SNe Ia	Redshift range
ESSENCE	2002–2007	102	0.1–0.78
SNLS	2003–2008	242	0.3–1.0
SDSS	2005–2007	448	0.05–0.4
Pan-STARRS	2009–2014	~ 3300	0.03–0.65
DES	2013–2018	~ 4000	0.05–1.2
J-PAS	2015–2021	~ 3800	0.05–0.4
LSST	2022–2032	~ 10000 per year	0.1–1.2

conclusions. In Appendix A we describe some usual transformations of an arbitrary function, for generic pedagogical reasons.

2. Fundamental quantities

The specific flux \mathfrak{F} (in the wavelength representation) measured by a detector is generically defined as the infinitesimal energy received by the detector per infinitesimal time interval, per infinitesimal perpendicular area, per infinitesimal wavelength interval,⁺ i.e.,

$$f_\lambda := \frac{dE}{dt dA_\perp d\lambda}. \quad (1)$$

The specific flux for a given source will in general depend not only on the wavelength λ , on the distance to the source r (cf. subsection 3.1) and on the source’s specific power or luminosity L_λ , but also, for transient sources, on the time t , and for moving sources, on the redshift z (cf. subsection 3.2); concretely $f_\lambda = f_\lambda(\lambda, t, r, z, L_\lambda)$. For simplicity, in future references to this equation we may suppress one or more dependences in the function f_λ . More on the discussion present in this section can be found in classical astrophysics books such as [22].

There are basically two techniques used for detecting astronomical objects: spectroscopy and photometry. In spectroscopy one uses a spectrograph to decompose the incoming light into its different wavelength components and obtain a measure of the specific flux at a given time, i.e. the spectrum of the object. Despite the high

\mathfrak{F} The expression *specific* refers to quantities measured per unit wavelength (or frequency), while *bolometric* refers to quantities integrated over all wavelengths (or frequencies).

⁺ The typical unit of f_λ is $1 \text{ erg/cm}^2/\text{s}/\text{\AA}$, whereas for the corresponding frequency representation, $f_\nu(t, \nu) = cf_\lambda(t, c/\nu)/\nu^2$, it is $1 \text{ erg/cm}^2/\text{s}/\text{Hz} = 10^{23} \text{ Jy}$ (jansky).

spectral resolving power in wavelength ($R := \lambda/\Delta\lambda$, where $\Delta\lambda$ is the resolution of the spectrograph) provided by spectroscopy (a low to intermediate resolution spectrograph has R of the order 1000–10000, whereas state of the art high resolution ones can achieve $R \simeq 100000$), it demands more observation time per object and more expensive equipment. In figure 2, we show some spectra from typical SNe Ia.

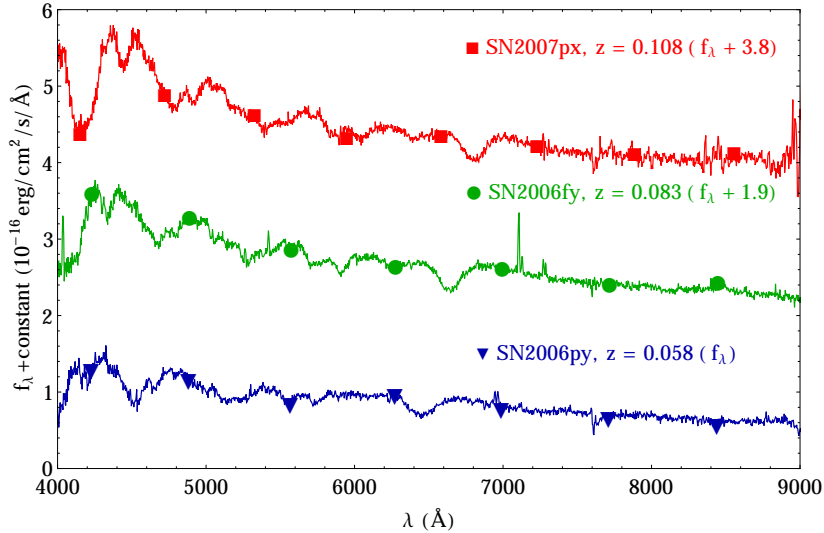


Figure 2. Observed spectra of some SNe Ia, at four days before B band maximum light.[23] Here and in all forthcoming figures showing spectra, geometric symbols (circles, squares, and triangles) serve only as a guide for the reader to better identify to which SN each curve refers.

In photometry one uses filters, which let the light pass only for a particular wavelength interval (the filter bandpass), and the resulting observation, called flux, corresponds to specific flux integrated over this interval. Flux measures in a given filter at different times (or epochs) constitute a usual (not specific) light curve of the object. Photometry is a cheaper and faster technique and there are many projects being designed to get a huge amount of data through photometric observations.

We now show how to obtain SN Ia light curve templates at a given filter from a theoretical model for $f_\lambda(\lambda, t)$. These templates are necessary for the standardization of SN Ia light curves, as will be discussed in section 4.

First we have to take into account the bandpass of the chosen filter. The filters $UBVRI$ (also known as the Johnson-Cousins filter set) are traditionally used to characterize SNe in the rest frame and will be used in this work. The reader can find a detailed discussion on photometric systems in Bessell.[24] We show in figure 3 the transmissivity curves, i.e. the fraction of energy that passes through the filter as a function of wavelength, S_λ^X , for these filters. It is important to notice that the filters are not perfect, in the sense that they do not let all photons pass, no matter what wavelength we consider. We will define the flux in band X , f^X , as the energy flux that

is transmitted through filter X , which can be written as

$$f^X(t) := \int_0^\infty f_\lambda(\lambda, t) S_\lambda^X(\lambda) d\lambda, \quad (2)$$

where we have, for brevity of notation, suppressed the dependence of f_λ (and thereby of f^X) on \mathbf{r} .

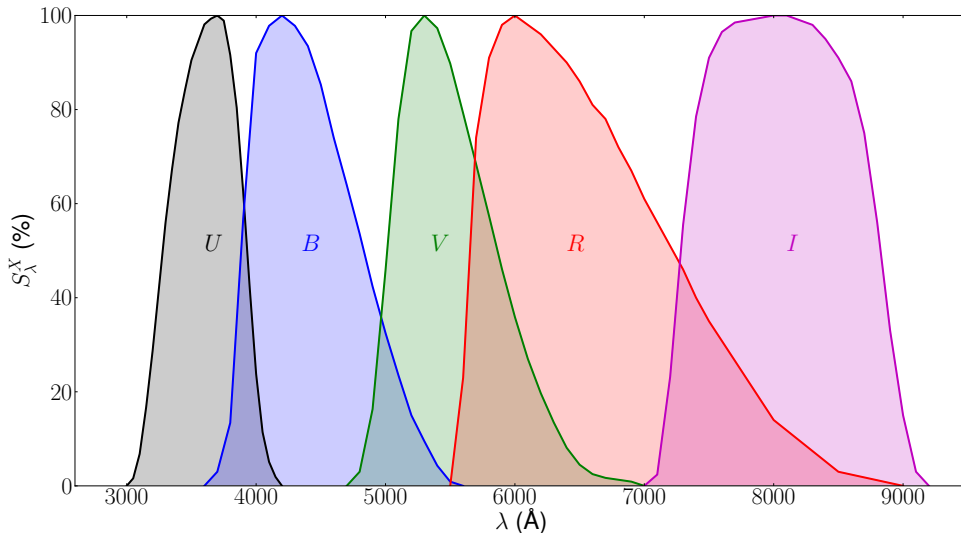


Figure 3. Transmissivity curves for the $UBVRI$ filters typically used in photometry.

The light curves are generally given in terms of the apparent magnitude in a given filter X , which is related to the flux f^X by*

$$m_X(t) := -2.5 \log \left(\frac{f^X(t)}{g^X} \right), \quad (3)$$

where g^X is the reference flux, that can be for instance the flux of a given star to which all other sources will be compared and defines a *magnitude system*. A *photometric system* is defined by a set of filters (in our case $UBVRI$) and the reference flux defined in all of them. In principle, the reference flux can be different for each filter, however this is not mandatory. In this work we use the AB magnitude system,[25, 26] which uses as reference a constant specific flux for all frequencies:

$$g_\nu^{AB} = 3631 \text{ Jy}.$$

Another commonly used magnitude system is the one that uses as reference flux the flux of the Vega star in the chosen filters. Our photometric system will be defined by the filter set $UBVRI$ and the AB magnitudes. In order to maintain the notation most commonly used by astronomers, throughout the text we are going to refer to the apparent magnitude in a given filter X by simply the letter X so, for example, the apparent magnitude of an object measured with the B filter will be just denoted B .

* Throughout the text \log denotes decimal (base 10) logarithm.

The filter reference flux g^X is given by

$$g^X := \int_0^\infty g_\lambda^X(\lambda) S_\lambda^X(\lambda) d\lambda, \quad (4)$$

where $g_\lambda^X(\lambda)$ is the specific reference flux for filter X .

Since we chose to perform our calculations in wavelength space, we need to rewrite the AB reference specific flux using the relation

$$g_\nu(\nu) d\nu = g_\lambda(\lambda) d\lambda.$$

Recalling that $c = \lambda\nu$, we can obtain the reference specific flux as a function of wavelength

$$g_\lambda^X(\lambda) = \frac{c g_\nu^{AB}}{\lambda^2}.$$

Therefore, to build a light curve, we need to evaluate the magnitudes for a given filter using (3) for spectra at different epochs. In figure 4, we show some light curves from typical SNe Ia, whereas in figure 5 we show a SN Ia light curve obtained from the SN Ia template generated by Nugent.[28]

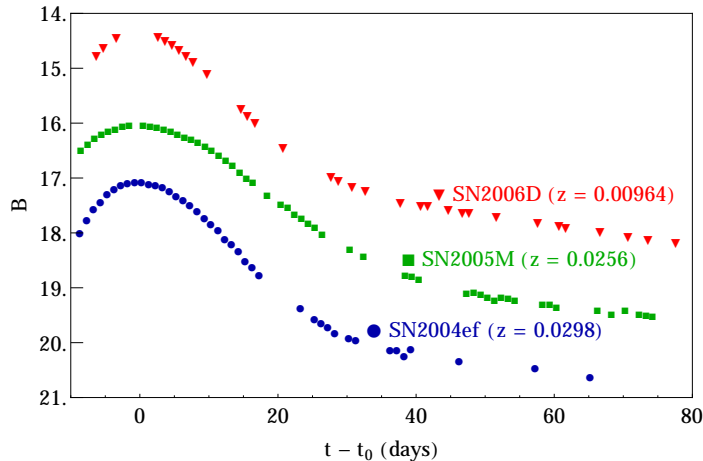


Figure 4. Observed sampling of apparent magnitude B band light curves from two Branch-normal (SN2004ef and SN2006D) and one 1991T-like (SN2005M) SNe Ia.[27] Notice that a simple visual inspection of the light curves does not allow determining the subtypes.

With given source and detector, we can display the visual representation of the function $f_\lambda(\lambda, t)$ by means of what we will call the spectral surface. In figure 6, for instance, we show a representation of this surface, constructed from Nugent's estimates based on real SNe Ia data,[28] for fixed z, r and L_λ (cf. section 3). The spectral surface displays in one single frame both the time evolution of the spectrum and the wavelength dependence of the specific light curve. The spectrum of the source, at a given time t_* , is the intersection of the spectral surface with the plane $t = t_*$, and the specific light curve, at a given wavelength λ_* , is the intersection of the spectral surface with the plane $\lambda = \lambda_*$. A spectral surface like the one shown in figure 6 would be the result of ideal

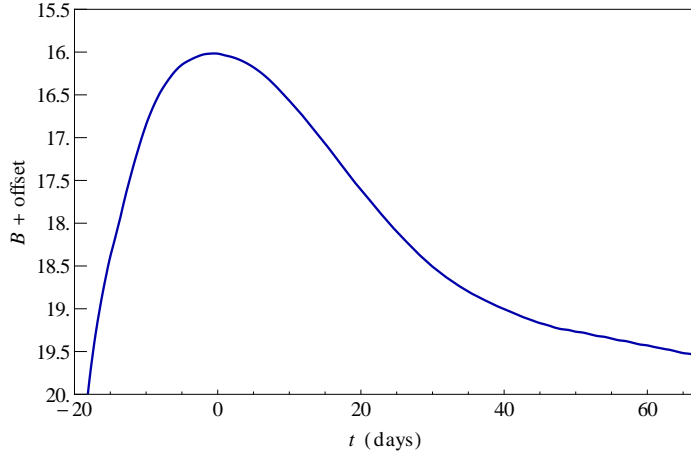


Figure 5. Theoretical B band light curve constructed from Nugent’s Branch-normal SN Ia spectral template.[28]

observations of a SN, continuous both in wavelength and time. In practice the best we can do is a discrete sampling of that surface for a given SN; however, even this would be unfeasible for a high number of SNe, because of the time demanded for the observations and the need for high cost facilities.

It is convenient to find a relationship between ideal detected quantities and intrinsic (source rest-frame) ones in a cosmological spacetime. To that end, as a motivating warm-up, let us consider an imaginary spherical (2-dimensional) surface, of radius R , concentric with a light source, both at rest in an inertial frame of the Minkowski spacetime. The bolometric (raw or pure) flux is defined as

$$f(t, R, L_\lambda) := \int_0^\infty f_\lambda(\lambda, t, R, L_\lambda) d\lambda, \quad (5)$$

and, due to conservation of energy, is trivially related to the intrinsic bolometric luminosity $L(t) := \int_0^\infty L_\lambda(\lambda, t) d\lambda$ by:

$$f(t, R, L) = \frac{L(t)}{4\pi R^2}. \quad (6)$$

We now introduce the concept of the redshift z , which is a measure of the relative velocity between astrophysical objects through the observation of their spectral features [29, 30]:

$$z := (\lambda_{obs} - \lambda_{em})/\lambda_{em},$$

where λ_{em} is the wavelength of a spectral feature, as measured in its rest frame, and λ_{obs} is the corresponding wavelength measured on Earth.

In Appendix B we show an intuitive way to obtain the relation between flux and luminosity for a more general spacetime, taking z into account, which is (B.4)

$$f_\lambda(\lambda, t, r, z, L_\lambda) = \frac{L_\lambda(\lambda/(1+z), t/(1+z))}{(1+z)^3 4\pi r^2}, \quad (7)$$

‡ Bolometric flux has the same units as band-limited flux: $1 \text{ erg/cm}^2/\text{s}$.

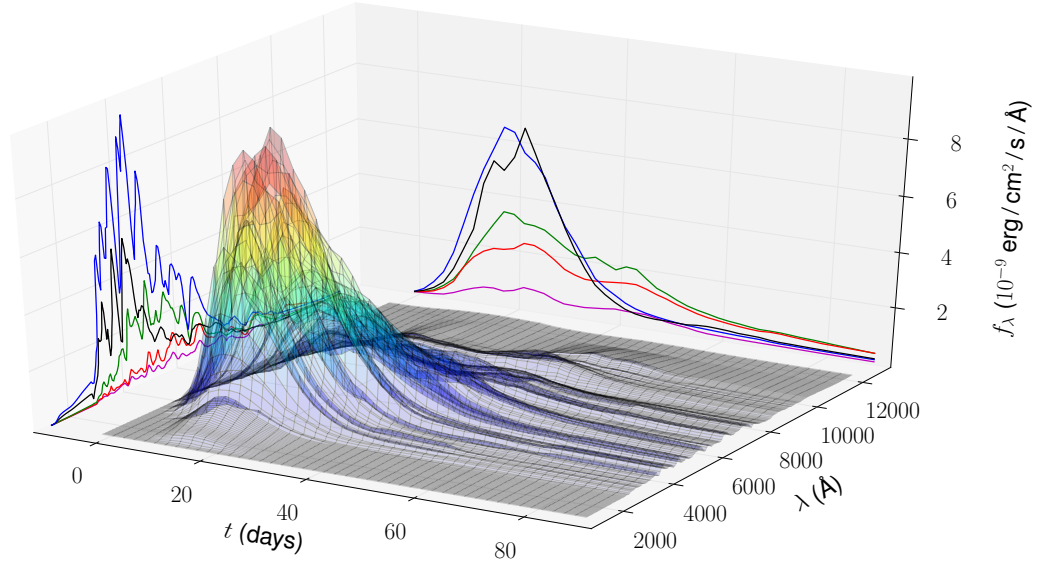


Figure 6. Theoretical rest-frame spectral surface generated from Nugent’s template of synthetic spectra, at different epochs or phases, of a typical Branch-normal SN Ia.[28] We also show five typical spectra, projected onto a conveniently offset plane $t = -10$ days, and five typical specific light curves, projected onto another conveniently offset plane $\lambda = 13000 \text{ \AA}$.

where $L_\lambda(\lambda/(1+z), t/(1+z))$ is the specific luminosity in the source’s rest-frame.

From specific flux measures in different wavelengths (or frequencies), in a given epoch, we can construct a spectrum of an astrophysical object. In figure 7, left panel, we show spectra of three SNe Ia, SN1994D,[31] SN1998aq[32] and SN2003du,[33] taken two days after maximum light (in B band, as we will see in the next sections), from the public database SUSPECT.[34] The characteristic shape of the spectral lines, known as P Cygni profile, indicates the presence of an expanding gas cloud. For a gas expanding with spherical symmetry, part of the light that is emitted toward us is coming from regions that are moving in our direction and is *blueshifted*, and the other part comes from regions that are moving away from us, being therefore redshifted. Since different layers of the expanding gas move with different velocities, the resulting spectrum presents wide emission lines centered at the rest wavelength value. As an example of such lines, we can see two SiIII absorption lines with rest-frame wavelengths $\lambda \approx 6347 \text{ \AA}$ and $\lambda \approx 6371 \text{ \AA}$ which appear in the spectrum in figure 7 as a broad absorption feature at $\lambda \approx 6150 \text{ \AA}$ (indicated by the dashed vertical line) followed by an emission line centered at $\lambda \approx 6350 \text{ \AA}$.

Based on the definition of apparent magnitude in a given filter, given by (3), we can introduce the concept of absolute magnitude, the apparent magnitude that the source

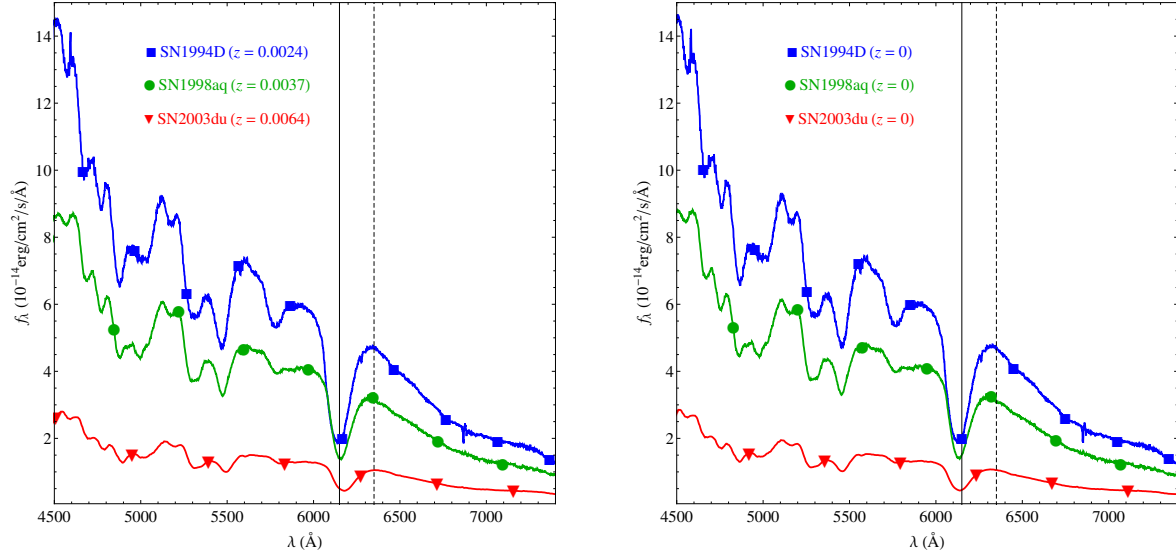


Figure 7. *Left panel:* spectra from Branch-normal SNe Ia 1994D, 1998aq and 2003du taken two days after maximum, in the B band. *Right panel:* same spectra in the SN Ia rest frame (cf. subsection 3.2). The vertical solid (dashed) lines indicate the typical rest-frame position of the absorption (emission) components for SiII, due to the P Cygni profile.

would have for a hypothetical observer at a distance of 10 parsecs^{††} and at rest with respect to it ($z = 0$),

$$M_X(t) := -2.5 \log \left(\frac{\int_0^\infty \frac{L_\lambda(\lambda, t)}{4\pi(10 \text{ pc})^2} S_\lambda^X(\lambda) d\lambda}{\int_{\lambda=0}^\infty g_\lambda^X(\lambda) S_\lambda^X(\lambda) d\lambda} \right). \quad (8)$$

We would like to call the reader's attention to the fact that, by its very definition, it makes no sense to refer to an absolute magnitude for $z \neq 0$, something that is not always explicit in the literature.

We can also consider an ideal case, in which we could measure the flux of a source in all wavelengths with a perfect detector ($S_\lambda^X(\lambda) = 1, \forall \lambda$), to define bolometric magnitudes,

$$m(t, z) := -2.5 \log \left(\frac{\int_{\lambda=0}^\infty f_\lambda(\lambda, t, z) d\lambda}{\int_{\lambda=0}^\infty g_\lambda(\lambda) d\lambda} \right), \quad (9)$$

$$M(t) := -2.5 \log \left(\frac{\int_{\lambda=0}^\infty \frac{L_\lambda(\lambda, t)}{4\pi(10pc)^2} d\lambda}{\int_{\lambda=0}^\infty g_\lambda(\lambda) d\lambda} \right). \quad (10)$$

^{††}The parsec is a distance unit frequently used in astronomy and corresponds to approximately 3.26 light-years or 3.08×10^{16} m. 1 parsec is the distance to an object with rest-frame size of 1 astronomical unit and apparent angular size of 1 arc second.

The distance to an astronomical object is directly related to its bolometric magnitudes through the quantity called *distance modulus*:

$$\mu := m - M. \quad (11)$$

As we will discuss in Section 3, the observed spectrum of a source is modified with respect to its intrinsic one by the redshift, and therefore the radiation emitted in a given wavelength range in the source's rest frame will be observed in a different range in the observer's frame. Also, since we simply cannot measure bolometric magnitudes, but only magnitudes in some filters, it is useful to express the distance modulus in terms of filter magnitudes, which requires the introduction of the so called *K-correction* K_{XY} defined as

$$K_{XY} := m_Y - M_X - \mu. \quad (12)$$

A full discussion of *K*-corrections and their applications for cosmology are left by the authors to another paper.

3. Dependence of specific flux on redshift and distance

It is important to note that even for a class of objects with the same intrinsic luminosity, which is approximately the case of SNe Ia (apart from the variations mentioned in section 1), their observed fluxes (both specific and bolometric) will differ mainly due to the different redshifts and distances.

From (B.4) we can see that, at a given time t and at a given wavelength λ , the specific flux can vary with distance r to the source, with redshift z , and with the functional form of the specific luminosity L_λ . Considering SNe Ia as standard candles means that we will assume all events to have the same specific luminosity. We know, however, that there are variations in their luminosities that should be taken into account and this will be considered in section 4. In the present section we will study how an arbitrary observed spectrum differs from the source's rest-frame spectrum, as we change, independently, the distance r and the redshift z . To that end, we advise the reader to refer now to Appendix A, where we graphically remind what happens to a function which is subjected to certain simple transformations that will be relevant in the next subsections.

3.1. Distance

Let us analyze first the simpler effect, the one arising from distance changes only. From (B.4), we can see the dependence of the specific flux on the inverse square of the distance r . Thus, when

$$r \longmapsto r' = cr \quad (c = \text{const.}), \quad (13)$$

all other independent variables held constant, we have that

$$f_\lambda(\lambda, t, r, z, L_\lambda) \longmapsto f'_\lambda(\lambda, t, r', z, L_\lambda) = c^{-2} f_\lambda(\lambda, t, r, z, L_\lambda). \quad (14)$$

Therefore, in a graph of the spectrum, as shown in figure 8 for SN1994D, we employ, in a linear scale (left panel), the vertical distortion of (A.3) and, in a logarithmic scale (right panel), the vertical translation of (A.1). The effect on the spectrum of a pure change only in distance is manifest in the logarithmic scale, where the rigid vertical translation is obvious.

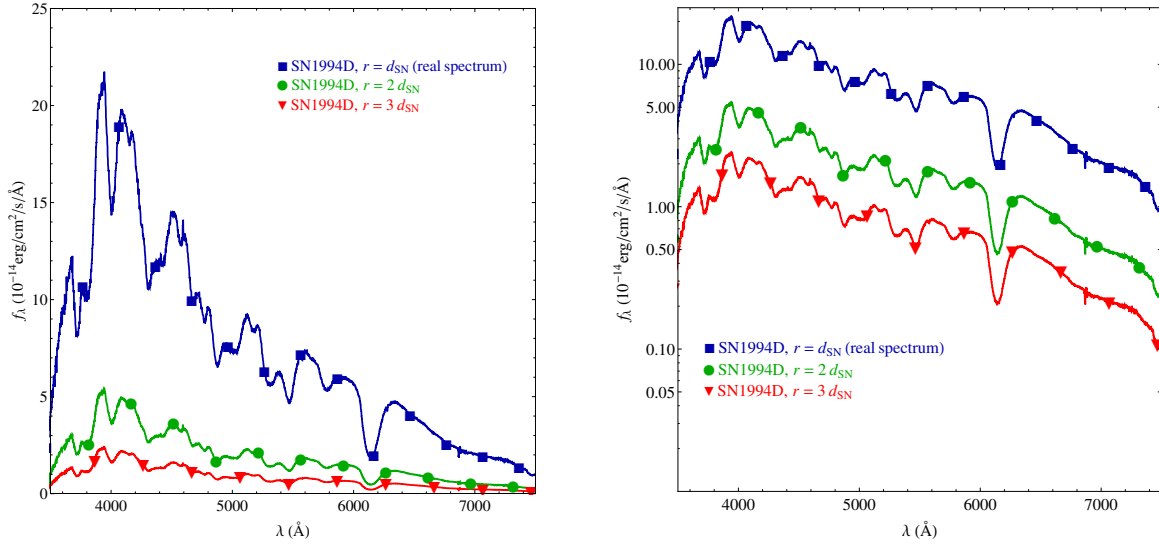


Figure 8. Synthetic spectra simulating the effect of distance on the spectrum of SN Ia 1994D, taken 2 days after maximum in the B band, in linear (left panel) and logarithmic (right panel) scales. The same spectrum was divided by different constants in order simulate different distances (cf. (B.4)).

3.2. Redshift

Let us analyze now the effect of the redshift, related to the relative motion between source and observer. Again, from (B.4), we can see the dependence of the specific flux on the inverse cube of $(1 + z)$ and also modifying explicitly the independent variables λ , and t by factors of $1/(1 + z)$. Thus, when

$$1 + z \mapsto 1 + z' = c(1 + z) \quad (c = \text{const.}), \quad (15)$$

all other independent variables held constant, we have that

$$f_\lambda(\lambda, t, r, z, L_\lambda) \mapsto f'_\lambda(\lambda, t, r, z', L_\lambda) = c^{-3} f_\lambda\left(\frac{\lambda}{c}, \frac{t}{c}, r, z, L_\lambda\right). \quad (16)$$

Of course, referring to the Appendix, we see that this transformation of the specific flux involves the composition of a vertical distortion, (A.3), and a horizontal distortion, (A.4). To get a handle on it more intuitively, let us choose $z = 0$ so that the former equation will provide the redshifted spectrum from the rest-frame one:

$$f'_\lambda(\lambda, t, r, z', L_\lambda) = \frac{1}{(1 + z')^3} f_\lambda\left(\frac{1}{1 + z'}\lambda, \frac{1}{1 + z'}t, r, z = 0, L_\lambda\right), \quad (17)$$

or vice versa, the rest-frame spectrum from the redshifted one:

$$f_\lambda(\lambda, t, r, z = 0, L_\lambda) = (1 + z')^3 f'_\lambda((1 + z')\lambda, (1 + z')t, r, z', L_\lambda). \quad (18)$$

Now, to illustrate this redshifting effect in a most pristine situation, we apply (17) to a top-hat function. The result is shown in figure 9. In the left panel, we show that the

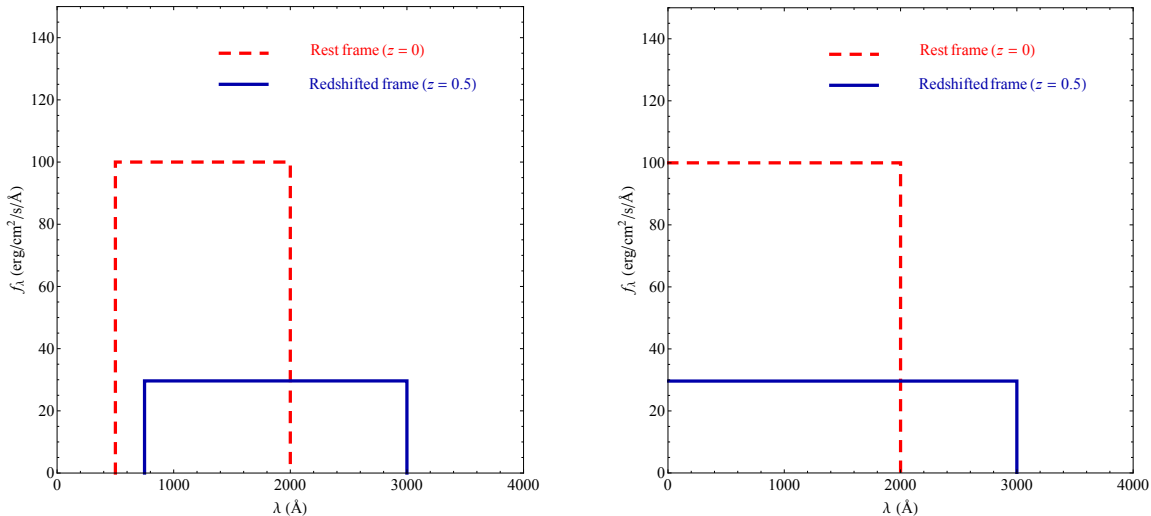


Figure 9. Effect of a variation in redshift on two top-hat spectra. The blue curve is the rest-frame spectrum ($z = 0$) and the red one is same spectrum at a redshift $z = 0.5$, in the observer’s frame.

total qualitative effect of the redshift is: (i) a vertical squeezing, due to the $1/(1 + z')^3$ pre-factor, and (ii) a horizontal stretch caused by the rescaling $\lambda \mapsto \lambda/(1 + z')$ in the first argument of f_λ . From this panel, the reader could naively be induced to regard the displacement towards greater wavelengths as a third, independent, effect; however, as can be seen from the right panel of figure 9, such a displacement is in fact also due to the horizontal stretch, which leaves the vertical y -axis ($\lambda = 0$) fixed (cf. (A.4) and right lower panel of figure A1).

In figure 7, left panel, we showed observed spectra of three SNe Ia. In its right panel, we now show the corresponding rest-frame ($z = 0$) spectra. We can notice the small horizontal displacement of the spectral lines (blueshifted, towards the left) but it is not possible to visualize the vertical displacement (upwards) due to the low values of the redshift involved. We can also see that, even after the redshift correction, the spectra do not coincide and this is because each SN is at a different distance from us.

To explicitly reveal the redshifting effect on the spectrum of a concrete SN Ia, we show, in figure 10, three spectra of SN 1994D, the rest-frame one and two other (artificial) high redshift ones (left panel). In particular, the effect of the pre-factor $1/(1 + z')^3$ in (17) can be best viewed using a logarithmic scale (right panel), in which it becomes a simple vertical translation (cf. (A.1) and left upper panel of figure A1).

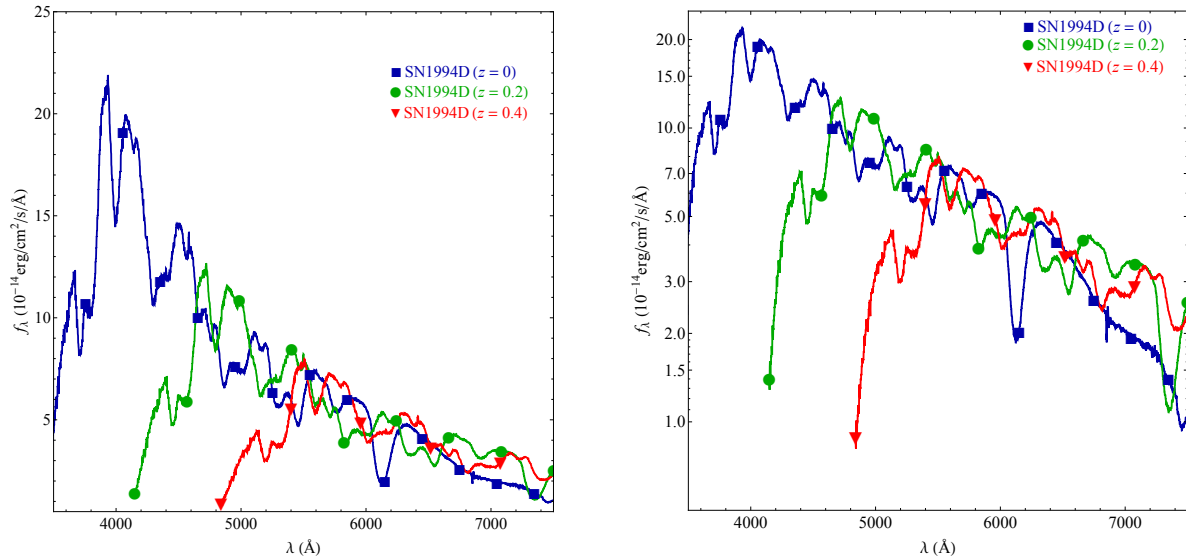


Figure 10. Synthetic spectra simulating the effect of redshift on the spectrum of SN Ia 1994D, taken 2 days after maximum in B band, for different values of redshift. We use a linear scale in the left panel and a logarithmic one in the right panel.

4. Light curve standardization

Although source-frame SNe Ia light curves are very similar, they are not identical. In this section we will show that it is possible to make them even more similar by applying some simple operations, which are dubbed standardization, and we will apply this procedure to a sample of real type Ia SNe. The process of standardization became possible after the discovery that intrinsically brighter SNe (at B band maximum) were also the ones with wider light curves.[35, 36] Such a correlation rendered it possible to determine if a given SN was brighter (fainter) than another one either because it was closer (further) or because it was intrinsically brighter (dimmer), just by looking at their light curves.

The data used in this work are publically available,[37] and constitute the sample of 85 low redshift SNe Ia observed by the Carnegie Supernova Project (CSP).[27, 38] Motivated by the higher uniformity of SNe Ia in the infra-red band, one of the main goals of that project was to obtain particularly well sampled and well characterized light curves both in optical and near-infrared bands, which should improve the efficiency of the standardization process. We restricted ourselves to the subsample of only Branch-normal SNe Ia, which reduced the number of events to 71. The corrections that we will present here were originally done simultaneously through a single fit that yields all the correction factors for each SN (cf. Goldhaber *et al.* [39]); however we chose to implement them step by step in order to make clear the role of each one in the final result.

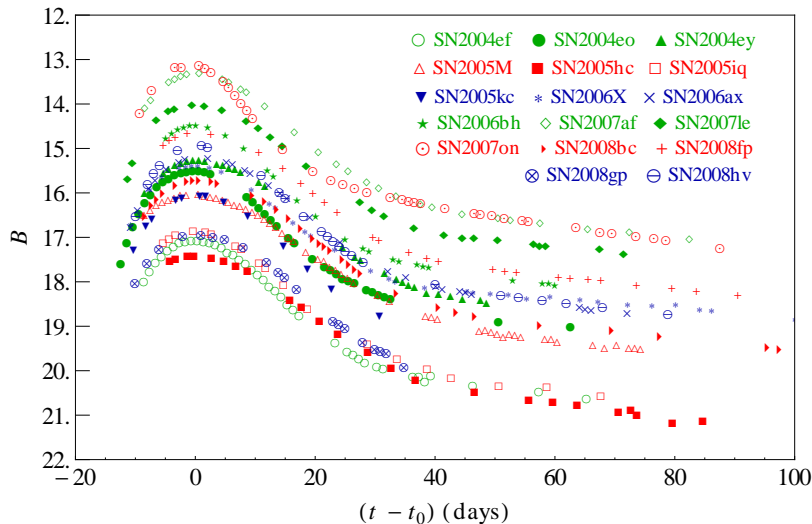


Figure 11. Apparent magnitude B band light curves of the 17 SNe Ia in our subsample after the time axis offset correction (cf. subsection 4.1).

4.1. Time axis offset correction

In the CSP light curve data, the epoch is expressed in Modified Julian Date (MJD). In order to compare them in a single plot, we need to define a common time scale $t - t_0$ [†], where t_0 is the epoch of maximum flux, traditionally considered in B band. We wrote a simple code to obtain t_0 for each supernova in our subsample. Unfortunately, some of them were observed only after B band maximum and were thus excluded from our subsample, which reduced considerably the number of SNe in the final subsample. In fact, we required our code to keep only the SNe that presented at least 3 observations taken before maximum flux and at least one observation taken after 30 days from maximum flux (the reason for this restriction will become clear in section 4.3). This left us with a subsample of 17 SNe, whose names and redshifts are listed in table 2, and whose time-offset-corrected light curves can be seen in figure 11.

4.2. Distance and redshift corrections

In order to properly standardize the light curves, we need to correct them for extrinsic effects. As we have seen in section 3, two of them can be easily taken account of: distance and redshift. The latter entails a change of the time scale and an offset to the magnitude (or change of the flux normalization) whereas the former implies a simple offset to the magnitude. Thus the correction for both effects amounts to:

- (i) a (horizontal) dilation, cf. (A.4), of the time axis such that

$$\frac{\Delta t_o}{\Delta t_e} = 1 + z, \quad (19)$$

[†] The time scale $t - t_0$ is commonly called *phase*.

Table 2. Names, CMB-centric redshifts and stretch factors (see section 4.3) for all 17 SNe Ia in the final subsample used to generate our simple light curve template.

	SN	z_{CMB}	s	s_G
1	2004ef	0.0298	0.89	0.81
2	2004eo	0.0147	0.87	0.88
3	2004ey	0.0146	1.14	1.00
4	2005M	0.0230	1.15	1.11
5	2005hc	0.0450	1.14	1.10
6	2005iq	0.0329	0.93	0.89
7	2005kc	0.0139	0.98	0.92
8	2006X	0.0063	1.01	0.93
9	2006ax	0.0179	1.12	0.98
10	2006bh	0.0105	0.86	0.82
11	2007af	0.0063	1.01	0.94
12	2007le	0.0055	1.12	0.97
13	2007on	0.0062	0.62	0.70
14	2008bc	0.0157	1.20	1.03
15	2008fp	0.0063	1.18	1.06
16	2008gp	0.0328	1.07	0.98
17	2008hv	0.0136	0.97	0.88

where Δt_o is a time interval in the observer’s frame and Δt_e is the corresponding interval in the source’s rest frame.

(ii) a (vertical) rigid translation, cf. (A.1), of the magnitude axis.

Notice that after the rigid vertical translations to correct for the redshift and distance, it is possible that the peaks of the light curves still do not coincide, since there can be absolute magnitude differences among them. So, in order to make the peaks coincide, a third vertical rigid translation is still needed. In our case, we do not know the distances to the SNe in our sample, so what we actually did was to evaluate the peak magnitude’s mean, and displace the light curves in order to make their magnitudes match this mean. This operation accounts for the rigid vertical translations due to both the redshift and the distance corrections, and also to a third rigid translation to correct for other differences in absolute magnitude.

The resulting distance- and redshift-corrected light curves of our subsample are shown in figure 12. In order to display all SNe in their rest frame time, notice that we have chosen to change the x -axis from $t - t_0$ to $(t - t_0)/(1 + z)$. Because of this, a little bit of care must be taken when comparing figure 12 and the following figures in this section to the results presented in section 3 and Appendix A, where we are keeping the x -axis unchanged before and after a given transformation.

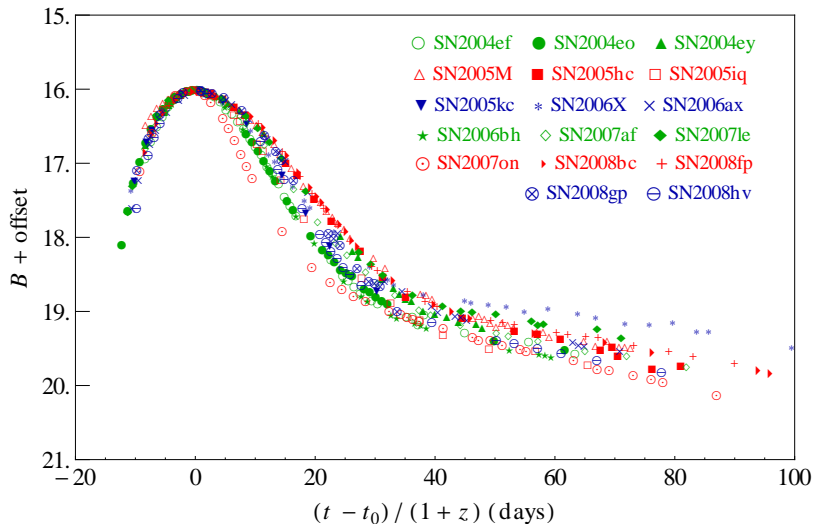


Figure 12. Apparent magnitude B band light curves + offset for the 17 SNe in our subsample after the time axis offset (cf. subsection 4.1) and distance and redshift corrections (cf. subsection 4.2).

4.3. The stretch correction

The stretch parameter s is related to the width of the light curve, i.e. it measures how fast the supernova’s flux decreases (or its magnitude increases). [12, 39] In order to calculate the stretch, we need to adopt a fiducial curve which, in our case, was chosen to be simply the mean of all curves in the sample, and assign the value $s = 1$ to it. A curve that declines slower (faster) than the fiducial one will have $s > 1$ ($s < 1$). After the corrections described in subsections 4.1 and 4.2 all curves coincide at the B band maximum but not necessarily at any other point. The stretch correction is designed so that the curves also coincide at 15 source frame days after B band maximum. We show a sketch of this procedure in figure 13, in which we use a fiducial (red curve) and two fictitious light curves, 1 and 2, in blue.

To obtain the stretch we need to solve for $p_i = (t - t_{0,i}) / (1 + z_i)$ from the following equation

$$f_i(p_i) = \bar{m}_{15}, \quad (20)$$

where f_i is an interpolating function (in our case a spline) for the i -th SN Ia B band light curve, and \bar{m}_{15} is the value of B (+ offset) of the mean light curve at $p_i = 15$ days. Thus, the stretch can be written as

$$s_i = \frac{p_i}{15 \text{ days}}. \quad (21)$$

We can then divide all phases of a supernova by the obtained stretch so the curves coincide at phase 15 days.

As mentioned earlier, the width difference in the light curves is associated to their intrinsic brightness (broader \leftrightarrow brighter). When we correct for the stretch we are compensating the differences in intrinsic brightness between the supernovae.

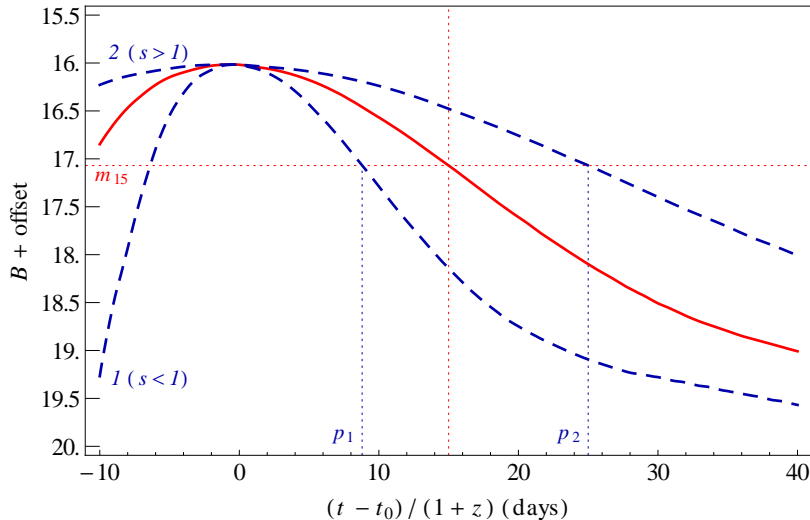


Figure 13. Schematics for stretch calculation. The red solid curve is the fiducial light curve, for which $s = 1$, by definition. The red dotted horizontal line indicates the position of m_{15} in the y -axis, which corresponds to the point in the fiducial curve where $(t - t_0)/(1 + z) = 15$ days, marked with the red dotted vertical line. The blue dashed curves are two other fictitious light curves, upon which we want to apply the stretch correction. The two blue dotted lines show the values of p for each curve, and the resulting range of the stretch factor is indicated near each curve.

The result of the application of the stretch procedure to our sample can be seen in figure 14. Table 2 shows the values of the stretch s found for each SN, according to our procedure. For comparison, we also show the values of the same parameter, now dubbed s_G , found using the method described in Goldhaber *et al.*, [39] where the corrections are all done simultaneously and the fiducial curve is different from ours. We can see that the results obtained with our step-by-step method agree quite well with the ones obtained with this more sophisticated fitting recipe.

4.4. The resulting template

After we apply all the corrections discussed above we can construct what we can call a “rudimentary” template, a simple mean of all corrected curves, that can be compared to the Nugent template, one of the most used in the literature. [28] We show the comparison in figure 15. In this comparison we can not use the relative discrepancy between these curves ($(B_N - \bar{B})/B_N$ or $(B_N - \bar{B})/\bar{B}$) because the normalizations of both are *arbitrary*. We can, on the other hand, compare the absolute difference shown in figure 15 (lower panel) to the range of the Nugent template in the depicted interval ($[-10, 30]$), for instance, which is 2.5, and the discrepancy thus calculated is always less than 12%. We can see that, despite the simplified analysis performed here, our curve looks quite similar to the template, which shows the consistency between our template and the Nugent one.

We show in figure 16 the standard deviation of our sample before and after the stretch correction. Again, we can not use relative discrepancies in the whole time

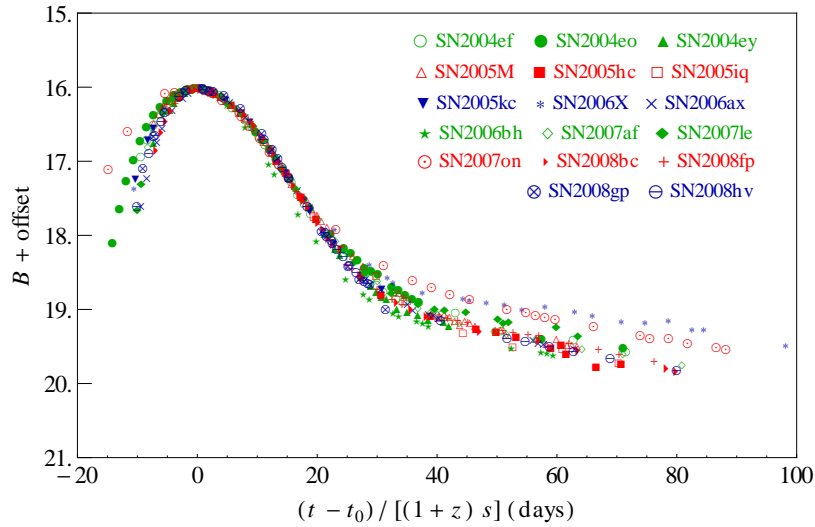


Figure 14. Apparent magnitude B band light curves + offset of the 17 SNe Ia in our subsample after the time axis offset (cf. subsection 4.1), distance and redshift (cf. subsection 4.2) and stretch corrections (cf. subsection 4.3). Note that the curves still present some dispersion, since the recipe imposes coincidence only at two points: $(t - t_0)/[(1 + z)s] = 0, 15$ days.

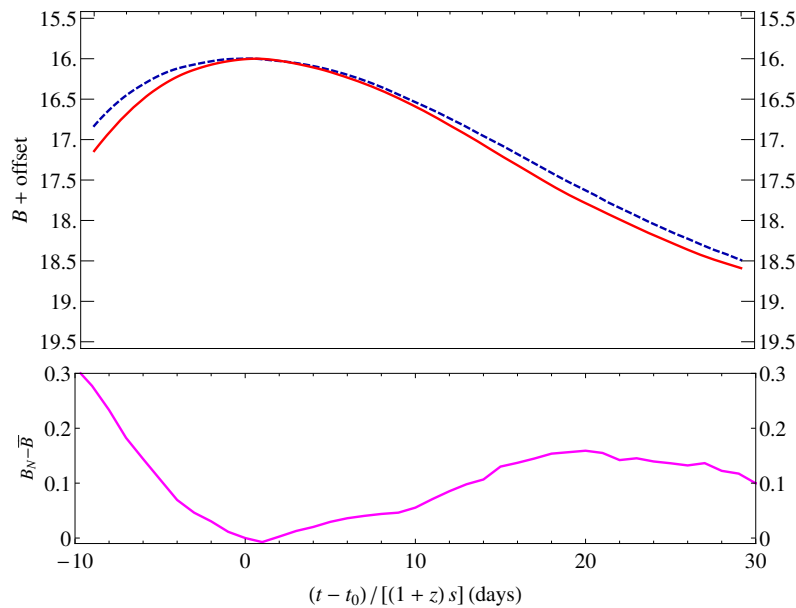


Figure 15. Comparison between our B band light curve template and Nugent's one.[28] Upper panel: B band rest-frame magnitude (arbitrarily normalized) versus rest-frame stretched phase for our template (red, solid curve) and for Nugent's one (blue, dashed curve). Lower panel: discrepancy between our template and Nugent's one.

interval to compare these curves because both the standard deviations are zero at $t - t_0 = 0$ by construction (see subsection 4.2) and the stretch corrected one is also null at $(t - t_0)/[s(1 + z)] = 15$. Nevertheless, the overall decreasing in the dispersion

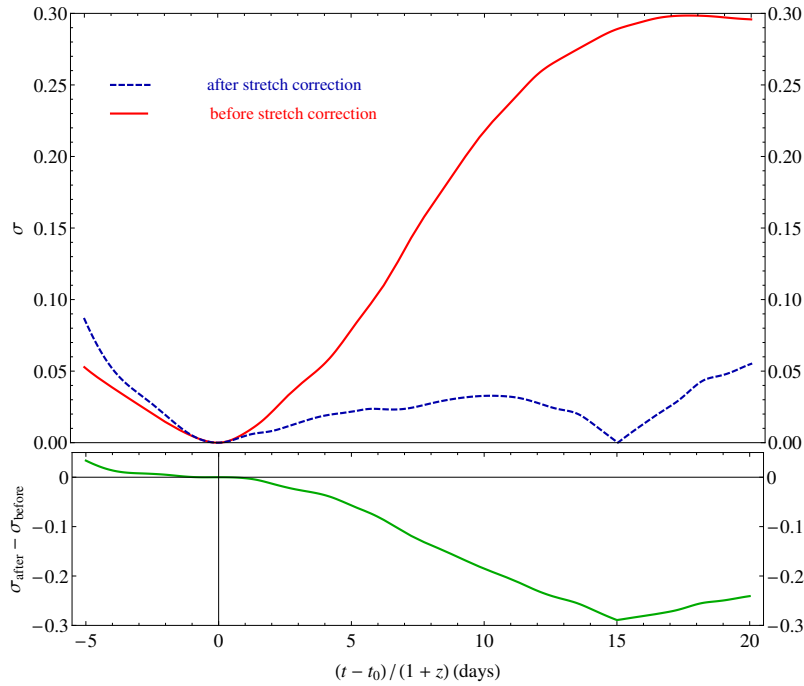


Figure 16. The role of the stretch correction in diminishing the dispersion. Upper panel: B band light curve standard deviation for the 17 SNe Ia after all corrections (blue, dashed curve), and with all but the stretch correction (red, solid curve). Lower panel: discrepancy between the standard deviations in magnitude of our subsample after all corrections (including the stretch one) and before the (last) stretch correction.

after the maximum is clear from figure 16 . Since such gain is obtained through a simple linear transformation, with only one parameter, we can argue that it reflects the homogeneity of the light curves in our sample

The reader might note that the discrepancy between the standard deviation after the stretch correction (in figure 16) is greater before maximum. This feature reflects the fact that the dispersion of the SNe Ia is smaller before the maximum (see Hayden *et al.*[40]). The stretch is defined to decrease the dispersion after maximum but it is applied to the whole light curve through (A.4) therefore, since the curves are more uniform before the maximum, when we multiply their arguments by different numbers the net result is an increasing of the dispersion in this interval.

5. Conclusion

This article had two main aims: (i) presenting and clarifying some fundamental concepts and results related to the cosmological use of SNe Ia, and (ii) building a simple SN Ia light curve template.

The first aim led us to introduce, in section 2, the specific flux or spectral energy distribution as the principal quantity characterizing the class of transient SNe Ia, and the corresponding projections (spectra and specific light curves). In section 3, we studied

in particular its dependence on distance and redshift and the consequent impact on the observed fluxes or magnitudes.

To comply with the second aim cited above, in section 4, we built our naive light curve template, for didactic purposes, through a simplified version of the original stretch procedure: we performed the determination of the three parameters of the method (the overall normalization of the light curve, the epoch of maximum flux in B band and the stretch itself) separately, instead of the simultaneous fit described in Goldhaber *et al.*[39] We finally constructed a mean light curve after the application of the method and compared it to a light curve template much used in the literature,[28] showing that our simplified method is able to produce a template very similar to it. In fact, the discrepancy is less than 10^{-2} for most of the phases in the interval of $[-10, 70]$ days in the light curve (see figure 15). From this very simple exercise we can infer how uniform the population of Branch-normal SNe Ia really is, since it is possible to decrease considerably the rest-frame magnitude standard deviation (after the maximum flux) of the light curves in our sample using just the single stretch parameter (cf. figure 16).

It is worth noting that after the discovery of the correlation between SN Ia luminosities and the width of their light curves, other secondary empirical correlations were also discovered, such as the one between a SN Ia luminosity and its color [41, 42] (the brightest SNe Ia are also the bluest ones). The process of standardization nowadays is, therefore, done through computational codes such as SALT2 [43] and MLCS2k2,[44] which take into account all these correlations.

Our current analysis does not yet address the relationship between the stretch parameter and the actual absolute value of the peak luminosity of SNe Ia, which is a necessary step for their use as extragalactic distance indicators. We leave this step for a future paper, which will take into account the cosmological applications of what has been presented here.

Acknowledgments

BBS would like to acknowledge financial support from the brazilian funding agency CAPES-PNPD, grant number 2940/2011.

Appendix A. Basic function transformations

In this Appendix we investigate four simple transformations (of one real parameter c on an arbitrary function $f : x \mapsto y = f(x)$ which bear upon the changes on the specific flux due to distance and redshift (cf. section 3). These are (cf. figure A1):

(i) *vertical translation* $T_{V,c}$:

$$T_{V,c}f : x \mapsto y := f(x) + c. \tag{A.1}$$

It always rigidly translates, along the vertical y -axis, the graph of the function f , by c “units”: upwards, if $c > 0$, and downwards, if $c < 0$.

(ii) *horizontal translation* $T_{H,c}$:

$$T_{H,c}f : x \longmapsto y := f(x + c). \quad (\text{A.2})$$

It always rigidly translates, along the horizontal x -axis, the graph of the function f , by c “units”: left, if $c > 0$, and right, if $c < 0$.

(iii) *vertical distortion* $D_{V,c}$:

$$D_{V,c}f : x \longmapsto y := cf(x). \quad (\text{A.3})$$

It always distorts, along the vertical y -axis, the graph of the function f , keeping a point with vanishing y coordinate fixed: if $|c| > 1$, it represents a dilation or stretch, the more so the larger $|c|$ is, whereas if $0 < |c| < 1$, it represents a contraction or compression, the more so the smaller $|c|$ is. Furthermore, if $c < 0$, this distortion is also accompanied by a reflection of the graph with respect to the x -axis.

(iv) *horizontal distortion* $D_{H,c}$:

$$D_{H,c}f : x \longmapsto y := f(cx). \quad (\text{A.4})$$

It always distorts, along the horizontal x -axis, the graph of the function f , keeping a point with vanishing x coordinate fixed: if $|c| > 1$, it represents a contraction or compression, the more so the larger $|c|$ is, whereas if $0 < |c| < 1$, it represents a dilation or stretch, the more so the smaller $|c|$ is. Furthermore, if $c < 0$, this distortion is also accompanied by a reflection of the graph with respect to the y -axis.

Appendix B. Obtaining the relation between specific flux and specific luminosity

Let us now proceed to the generalization of (5) to the Robertson-Walker spacetime, whose line element may be cast in the form:

$$ds^2 = -c^2 dt^2 + a(t)^2 \left[\frac{dr^2}{1 - kr^2} + r^2 (d\theta^2 + \sin^2 \theta d\varphi^2) \right], \quad (\text{B.1})$$

where k is the spatial curvature and $a(t)$ is the dimensionless scale factor. The coordinate r is variously called the comoving areal distance, transverse comoving distance or proper motion distance.[45, 46]

We first deal with the traditional case in which source and detector are both in the Hubble flow, so that their relative velocity is all due to the cosmic expansion, and is traditionally called a recession velocity. In this case, time intervals dt_S in the source’s rest-frame, such as the time between the emission of two consecutive photons, correspond to time intervals in the detector’s frame $dt_D = (1 + \bar{z}) dt_S$, where \bar{z} is the usual cosmological redshift: $1 + \bar{z} = 1/a(t)$. The source-frame and detector-frame energies of the photon will also be related by a factor $(1 + \bar{z})$. Therefore, assuming conservation of photons, the bolometric flux of a source at cosmological redshift \bar{z} can be written as

$$f(t, r, \bar{z}, L) = \frac{L(t/(1 + \bar{z}))}{4\pi r^2 (1 + \bar{z})^2}, \quad (\text{B.2})$$

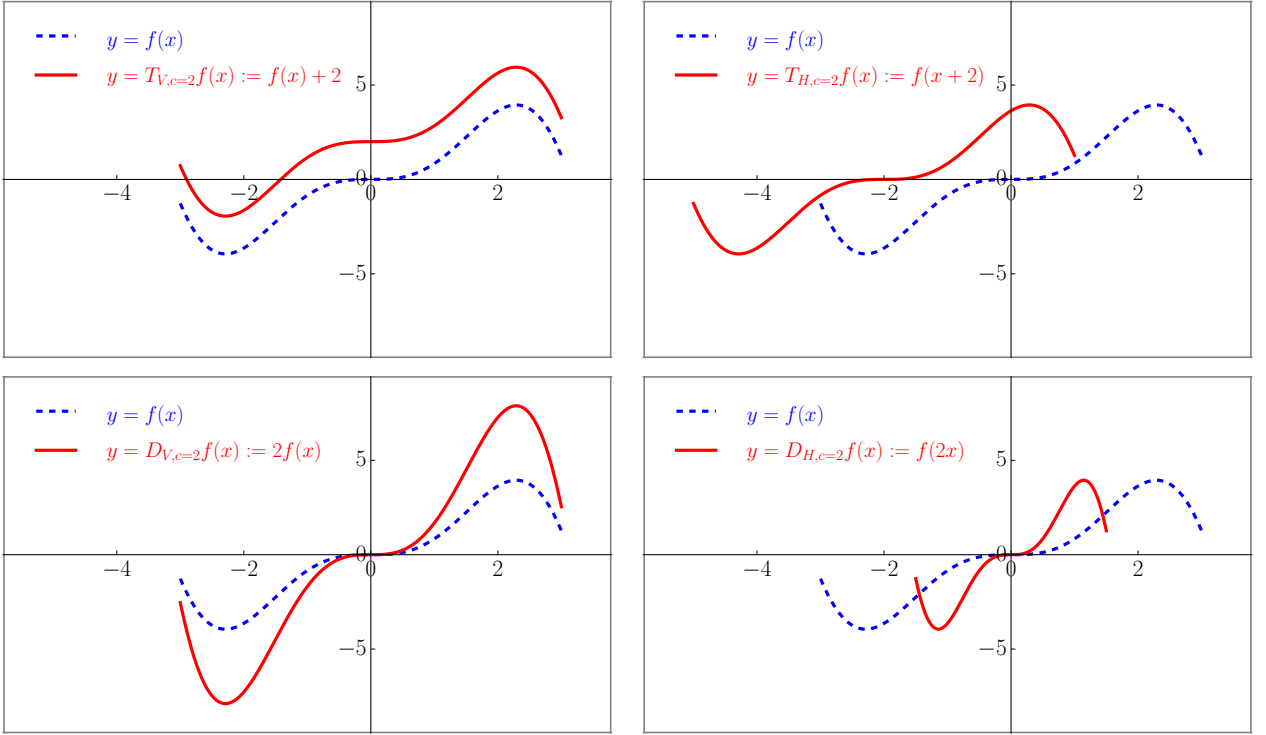


Figure A1. Basic transformations of a given arbitrary function f : the original graph is represented by a (blue) dashed line and the transformed graph by a (red) solid line. Left upper panel displays the effect of a vertical translation $T_{V,c}$ with $c = 2$. Right upper panel displays the effect of a horizontal translation $T_{H,c}$ with $c = 2$. Lower left panel displays the effect of a vertical distortion $D_{V,c}$ with $c = 2$. Lower right panel displays the effect of a horizontal distortion $D_{H,c}$ with $c = 2$.

where t is a time coordinate measured with respect to a reference time t_R which, for simplicity, we choose to be $t_R = 0$ in both frames. In this way, a time interval $t - t_R = t$ in the observer's frame corresponds to the interval $(t - t_R)/(1 + \bar{z}) = t/(1 + \bar{z})$ in the source's rest-frame.

Finally, we state that an equation of this same form holds for an arbitrary motion (not in the Hubble flow) of the source and the detector, viz.,

$$f(t, r, z, L) = \frac{L(t/(1+z))}{4\pi r^2(1+z)^2}, \quad (\text{B.3})$$

where now z is the total redshift between the source and the detector, which is the really observed one[‡] Since the specific flux is related to the bolometric one by (5), it is obvious

[‡] This demonstration, besides some alternative definitions of luminosity distance, and its consequences for SNe Ia, will be explored in a forthcoming paper, in preparation.

that it can be expressed as

$$f_{\lambda}(\lambda, t, r, z, L_{\lambda}) = \frac{L_{\lambda}(\lambda/(1+z), t/(1+z))}{(1+z)^3 4\pi r^2}, \quad (\text{B.4})$$

where $L_{\lambda}(\lambda/(1+z), t/(1+z))$ is the specific luminosity in the source's rest-frame.

We can also obtain the frequency representation of the specific flux as

$$f_{\nu}(\nu, t, r, z, L_{\nu}) = \frac{L_{\nu}(\nu(1+z), t/(1+z))}{(1+z) 4\pi r^2}. \quad (\text{B.5})$$

We can obtain (6) by integrating either B.4) on λ or (B.5) on ν .

References

- [1] Hoyle F and Fowler W A 1960 Nucleosynthesis in Supernovae *Astrophys. J.* **132** 565.
- [2] Padmanabhan T 2001 Theoretical astrophysics II: stars and stellar systems (Cambridge: Cambridge University Press).
- [3] Chandrasekhar S 1931 The maximum mass of ideal white dwarfs *Astrophys. J.* **74** 81–82.
- [4] Diemer B, Kessler R, Graziani C, Jordan G C IV, Lamb D Q, Long M and van Rossum D R 2013 Comparing the light curves of simulated type Ia supernovae with observations using data-driven models *Astrophys. J.* **773** 119.
- [5] Hillebrandt W, Kromer M, Röpke F K and Ruiter A J 2013 Towards an understanding of type Ia supernovae from a synthesis of theory and observations *Front. Phys.* **8** 116.
- [6] Maoz D, Mannucci F and Nelemans G Observational clues to the progenitors of type Ia supernovae arXiv:1312.0628; to appear in *Ann. Rev. Astron. Astrophys.*
- [7] Filippenko A V 1997 Optical spectra of supernovae *Ann. Rev. Astron. Astrophys.* **35** 309.
- [8] Branch D, Fisher A and Nugent P 1993 On the relative frequencies of spectroscopically normal and peculiar type IA supernovae *Astron. J.* **106** 2383.
- [9] Vaughan T E, Branch D, Miller D L and Perlmutter S 1995 The blue and visual absolute magnitude distributions of type Ia supernovae *Astrophys. J.* **439** 558.
- [10] Richardson D, Jenkins III R L, Wright J and Maddox L 2014 Absolute-magnitude distributions of supernovae *Astron. J.* **147** 118.
- [11] Riess A G *et al* 1998 Observational evidence from supernovae for an accelerating universe and a cosmological constant *Astron. J.* **116** 1009.
- [12] Perlmutter S *et al* 1999 Measurements of Ω and Λ from 42 high-redshift supernovae *Astrophys. J.* **517** 565.
- [13] Kunz M 2012 The phenomenological approach to modeling the dark energy *Comptes rendus - Physique* **13** 539.
- [14] Dilday B *et al* Measurements of the rate of type Ia supernovae at redshift $z \lesssim 0.3$ from the SDSS-II Supernova Survey *Astrophys. J.* **713** 1026.
- [15] Miknaitis G *et al* 2007 The ESSENCE Supernova Survey: Survey Optimization, Observations, and Supernova Photometry *Astrophys. J.* **666** 674.
- [16] Conley A *et al* 2011 Supernova Constraints and Systematic Uncertainties from the First 3 Years of the Supernova Legacy Survey *ApJS* **192** 1.
- [17] Sako M *et al* 2014 The Data Release of the Sloan Digital Sky Survey-II Supernova Survey arXiv:1401.3317.
- [18] Rest A *et al* 2013 Cosmological Constraints from Measurements of Type Ia Supernovae discovered during the first 1.5 years of the Pan-STARRS1 Survey arXiv:1310.3828.
- [19] Bernstein J *et al* 2012 Supernova Simulations and Strategies For the Dark Energy Survey *Astrophys. J.* **753** 152.
- [20] Benitez N *et al* 2014 J-PAS: The Javalambre-Physics of the Accelerated Universe Astrophysical Survey arXiv:1403.5237.

- [21] Abell P A *et al* 2009 LSST Science Book, Version 2.0 arXiv:0912.0201.
- [22] Carroll B W and Ostlie D A 2006 *An Introduction to Modern Astrophysics* (San Francisco: Pearson-Addison-Wesley).
- [23] Östman L *et al* 2011 NTT and NOT spectroscopy of SDSS-II supernovae *Astron. Astrophys.* **526** A28.
- [24] Bessell S 2005 Standard photometric systems *Ann. Rev. Astron. Astrophys.* **43** 293.
- [25] Oke J B 1965 Absolute spectral energy distributions in stars *Ann. Rev. Astron. Astrophys.* **3** 23–46.
- [26] Oke J B and Gunn J E 1983 Secondary standard stars for absolute spectrophotometry *Astrophys. J.* **266** 713.
- [27] Contreras C *et al* 2010 The Carnegie Supernova Project: first photometry data release of low-redshift type Ia supernovae *Astron. J.* **139** 519–539.
- [28] Peter Nugent templates, <http://supernova.lbl.gov/~nugent/nugent_templates.html>.
- [29] Synge J L 1960 *Relativity: the general theory* (Amsterdam: North-Holland,).
- [30] Narlikar J V 1994 Spectral shifts in general relativity *Am. J. Phys.* **62** 903.
- [31] Patat F, Benetti S, Cappellaro E, Danziger I J, della Valle M, Mazzali P A and Turatto M 1996 The type IA supernova 1994D in NGC 4526: the early phases *Mon. Not. Royal Astron. Soc.* **278** 111.
- [32] Branch D, Garnavich P, Matheson T, Baron E, Thomas R C, Hatano K, Challis P, Jha S and Kirshner R P 2003 Optical spectra of the type Ia supernova 1998aq *Astron. J.* **126** 1489.
- [33] Gerardy C L 2005 *1604-2004: Supernovae as cosmological lighthouses* ASP Conference Series **342** edited by Turatto M, Benetti S, Zampieri L and Shea W (San Francisco: Astronomical Society of the Pacific) p 250.
- [34] SUSPECT Web Site, <<http://nhn.nhn.ou.edu/~suspect/>>.
- [35] Phillips M M 1993 The absolute magnitudes of type Ia supernovae *Astrophys. J.* **413** L105.
- [36] Hamuy M, Phillips M M, Schommer R A, Suntzeff N B, Maza J and Avilés R 1996 The absolute luminosities of the Calán/Tololo type Ia supernovae *Astron. J.* **112** 2391.
- [37] Carnegie Supernova Project Web Site, <<http://csp.obs.carnegiescience.edu/data>>.
- [38] Stritzinger M D *et al* 2011 The Carnegie Supernova Project: second photometry data release of low-redshift type Ia supernovae *Astron. J.* **142** 156.
- [39] Goldhaber G *et al* 2001 Timescale stretch parameterization of type Ia supernova *B*-band light curves *Astrophys. J.* **558** 359.
- [40] Hayden B T *et al* 2010 The rise and fall of type Ia supernova light curves in the SDSS-II Supernova Survey *Astrophys. J.* **712** 350–366.
- [41] Lira P, Masters thesis, University of Chile.
- [42] Riess A G, Press W H and Kirshner R P 1996 A Precise Distance Indicator: Type IA Supernova Multicolor Light-Curve Shapes *Astrophys. J.* **473** 88.
- [43] Guy J *et al* 2007 SALT2: using distant supernovae to improve the use of Type Ia supernovae as distance indicators *Astron. Astrophys.* **466** 11–21.
- [44] Jha S, Riess A G and Kirshner R P 2007 Improved Distances to Type Ia Supernovae with Multicolor Light Curve Shapes: MLCS2k2 *Astrophys. J.* **659** 122.
- [45] Weinberg S 1972 *Gravitation and cosmology: principles and applications of the general theory of relativity* (New York: John Wiley & Sons).
- [46] Hogg D W 1999 Distance measures in cosmology arXiv:astro-ph/9905116.